Published in Metallurgical and Materials Transactions A

Microstructure, texture and superplasticity of a fine-grained Mg–Gd–Zr alloy processed by equal-channel angular pressing

R. Alizadeh [a,b], R. Mahmudi [a,*], A.H.W. Ngan [b], P.H.R. Pereira [c], Y. Huang [c], T.G. Langdon [c]

[a] *School of Metallurgical and Materials Engineering, College of Engineering, University of Tehran, Tehran 14399-57131, Iran.*

[b] *Mechanical Engineering Department, The University of Hong Kong, Pokfulam Road, Hong Kong.*

[c] *Materials Research Group, Faculty of Engineering and the Environment, University of Southampton, Southampton SO17 1BJ, U.K.*

*Corresponding author: e-mail: mahmudi@ut.ac.ir, Phone: +98 21 8208 4137, Fax: +98 21 8800 6076

ABSTRACT

There are limited reports to date on the microstructure and superplasticity of the Mg–Gd alloys after processing by equal-channel angular pressing (ECAP). Accordingly, the effects of ECAP temperature of 473 to 723 K (200 to 450 ^{o}C) and number of passes (2, 4 and 8) on the microstructure and texture of an extruded Mg–5Gd–0.4Zr (GW50) alloy were investigated by SEM, TEM and EBSD. The results show that the optimum ECAP temperature is 623 K (350 ^{o}C). Higher temperatures give extensive grain growth and the material has insufficient formability at lower temperatures. The results show also that the alloy exhibits no further grain refinement after four ECAP passes and there is slight grain growth at 8 ECAP passes. Samples were processed by four passes at 623K (350 ^{o}C) and then subjected to shear punch testing. The results confirm the occurrence of superplastic behavior at 723 K (450 ^{o}C) with a maximum strain rate sensitivity index of ~ 0.47 and an activation energy of ~110 kJ mol^{-1}. The results are consistent with the occurrence of flow by grain boundary sliding in the superplastic region.

Keywords: ECAP; Mg–Gd–Zr alloy; Shear punch test; Superplasticity; Texture

I. INTRODUCTION

Magnesium alloys have been the subject of much research in recent years due to their low density, high specific strength and stiffness combined with their reasonable cost. Despite these advantages, Mg alloys suffer from poor formability at low temperatures because of the limited slip systems in their hexagonal close-packed (hcp) crystal structure.[1] There are two basic methods for improving the formability of Mg alloys; the first is to use severe plastic deformation (SPD) processes to achieve greater grain refinement and the second is to increase the forming temperature. Superplasticity refers to the ability of a material to undergo extensive plastic deformation and this can be achieved at high temperatures in fine-grained materials processed using SPD techniques.[2] However, there are limitations associated with heating simple magnesium alloys to high temperatures because the microstructures of fine-grained alloys tend to be unstable and exhibit extensive grain growth. Accordingly, attempts have been made to improve their thermal stability through the addition of different alloying elements and in this respect it was reported that the addition of gadolinium (Gd) and other rare earth (RE) elements leads to a remarkable improvement in the thermal stability of the microstructure, and in the mechanical properties at high temperatures, due to solution and precipitation hardening.[3,4]

Excellent thermal stability of Mg–Gd alloys has permitted the occurrence of extensive superplasticity in these alloys. Table 1 provides a comprehensive summary of the investigations reported to date for superplastic flow in various Mg–Gd alloys:[5–14] in this table, the SPD processing conditions are listed in columns 2 to 3, the resultant grain sizes are listed in column 4 and the superplastic testing conditions are given in columns 5 to 7, where data are included only when the maximum elongations exceed the critical requirement of a tensile elongation of at least 400 pct for superplastic flow and/or a strain rate sensitivity (SRS) index exceeding 0.40.[15] It is readily apparent from inspection of Table I that these alloys generally exhibit excellent superplastic properties with a maximum elongation of 3570 pct reported for an Mg–9.4Gd–

4.1Y–1.2Zn–0.4Zr alloy.[9] Nano-sized grains also were achieved in an Mg–9Gd–4Y–0.4Zralloy (GW94) after processing by high pressure torsion (HPT) at room temperature.[14] Nevertheless, most investigations have used simple extrusion methods for producing fine-grained materials and there is only one report where superplasticity was documented in an Mg–Gd alloy processed by equal-channel angular pressing (ECAP).[12] Also, there are only limited numbers of reports to date on the microstructural evolution in Mg–Gd alloys after ECAP.[16,17] Hence, the objective of the present investigation was to study the microstructural evolution and superplasticity in an extruded

Mg–5Gd–0.4Zr alloy after processing through different ECAP conditions and thereby to identify the optimum ECAP parameters for achieving grain refinement and superplasticity.

Although tensile testing is the conventional standard procedure for delineating superplasticity, localized testing methods are now available for measuring the strain rate sensitivity and thus providing an indirect method for identifying the possible occurrence of superplastic flow through the use of smaller samples. Different techniques have been successfully used for investigating superplasticity in different materials. A summary of the different localized methods used to evaluate the occurrence of superplasticity in different materials is given in Table II.[11,13,14,18–22] It can be observed from Table II that shear punch testing (SPT) has been used recently as a suitable technique for measuring the SRS in different materials processed by SPD methods. Therefore, SPT was used in the present investigation in order to evaluate the occurrence of superplasticity.

II. EXPERIMENTAL

The material used in this investigation was an Mg–5 wt pct Gd–0.4 wt pct Zr (GW50) alloy which was prepared from high purity Mg, Mg–30Gd and Mg–30Zr master alloys by melting in an electrical furnace under the protective MAGREX 36* flux cover. Extrusion was conducted at

* MAGREX 36 is a trade mark of Foseco, Staffordshire, United Kingdom.

a ratio of 8:1 at 673 K (400 ^{o}C). Round ECAP billets with diameter of 10 mm and length of 65 mm were machined from the extruded bars. The processing by ECAP was conducted at temperatures of 473 K (200 ^{o}C), 573 K (300 ^{o}C), 623 K (350 ^{o}C) and 723 K (450 ^{o}C), with strain rate of about 0.05 s^{-1} and using route B_c, where each billet is rotated longitudinally by 90° in the same sense between passes.[23] The ECAP die contained a die angle of 90° and an outer arc of curvature of 20° so that each pass imposed a strain of ~1[24][24] and the processing was performed through 2, 4 or 8 passes whenever the material showed sufficient formability.

Slices of ~1 mm thickness were cut from the samples perpendicular to the extrusion direction (ED) for microstructural characterization. A Hitachi S-3400N variable pressure scanning electron microscope (SEM) and a Hitachi S-4800 field emission gun scanning electron microscope (FESEM) were used for microstructural characterization. The samples for the SEM investigations were etched with an acetic-picral solution. An FEI Tecnai G2 20 S-TWIN scanning transmission electron microscope (TEM) with a maximum operating voltage of 200 kV was also used for determining the crystal structure and chemical composition of the precipitates. TEM samples were cut by punching. After grinding the samples to ~100 μm thickness, their thicknesses were further reduced to ~20 μm with a dimpler machine and the TEM samples were finally prepared by ion beam milling using a milling angle of 12° with a voltage of 4 kV. Electron backscattered diffraction (EBSD) was used to study the orientation maps and texture evolution. The specimen preparation for EBSD involved SiC paper grinding and diamond paste polishing, followed by vibratory polishing with an alcohol-based alumina.

SPT was used for the evaluation of superplasticity after optimum ECAP conditions, where full details of the SPT technique were given earlier.[25] The SPT was performed at temperatures of 623 K (350 ^{o}C), 673 K (400 ^{o}C), 723 K (450 ^{o}C) and 773 K (500 ^{o}C) under shear strain rates in the range from 1.7×10^{-2} to 2.7×10^{-1} s^{-1} using a screw-driven MTS testing system equipped

105 with a three-zone split furnace. A shear punch fixture with a 2.957 mm diameter flat cylindrical
106 punch and 3.044 mm diameter receiving hole was used for SPT. Thin slices with 0.9 mm
107 thickness were cut by electro-discharge machining perpendicular to the ED. Both sides of these
108 discs were ground with SiC abrasive paper (grade 800) to a thickness of about 0.7 mm in order to
109 remove the surface roughness. These samples were placed at the center of the SPT die which
110 means the shear deformation was performed at a radius of ~1.5 mm from the center of the discs.
111 The load, F, was measured automatically as a function of the punch displacement and the data
112 were recorded by appropriate software to determine the shear stress, τ, on the tested material
113 using the relationship[26]

114 $$\tau = \frac{F}{\pi D t} \qquad (1)$$

115 where t is the specimen thickness and D is the average of the punch and die hole diameters. To
116 eliminate the slight differences between the thicknesses of the SPT samples, the measured
117 displacements were normalized to the initial thicknesses of the discs. The SPT curves were then
118 plotted as shear stress against normalized punch displacement.
119
120 ## III. RESULTS
121 ### *A. Microstructural and textural evolution*
122 SEM micrographs of the alloy after extrusion are shown in Figure 1. As can be observed, the
123 material does not show a uniform grain size structure and some large grains are detected in the
124 microstructure. Therefore, the grain size distribution in the extruded condition is bimodal
125 comprising a mixture of fine grain (FG) and coarse grain (CG) zones. The average grain size of
126 the FG zone was about 5.5 ± 0.5 μm.
127 Another important feature of the microstructure of the alloy in the extruded condition was
128 the presence of some cuboid precipitates. While most of these precipitates were located at the

grain boundaries, some particles also were formed within the grains (Figure 2). Energy dispersive X-ray spectrometry (EDS) line scan results, shown in Figure 2, indicate that these particles are rich in Gd. To understand the crystal structure and chemical composition of the cuboid precipitates some of them were subjected to selected area electron diffraction (SAED) and EDS analysis by TEM. The results are shown in Figures 3 and 4 for one of such precipitates. This particle is cuboid in shape (Figure 3a), with dimensions of about 780 nm × 1200 nm. The SAED results, shown in Figure 3b and 3c, indicate that the crystal structure can be indexed as a face-centered cubic (fcc) structure with a lattice parameter of 0.53 nm. Similar results were obtained for two other cuboid precipitates. The TEM-EDS spectra for points *A* (surrounding Mg matrix) and *B* (cuboid precipitate) are shown in Figure 4a and 4b and the results are summarized in Figure 4c. It can be observed that the cuboid precipitate is rich in Gd, and the Gd/Mg ratio (in atomic percentage) is close to 1.8. It would be helpful now to compare the determined crystal structure with those reported before for similar RE-rich cuboid precipitates in the Mg-RE alloys. In some studies, this phase has been shown to have an fcc crystal structure with a lattice parameter of 0.54–0.56 nm and chemical composition close to Mg_5RE.[27-31] However, there are later reports which show that the fcc phase can be identified as RE hydrides, such as REH_2.[32-35] In this regard, it has been recently proposed that the RE hydrides are probably formed as a result of the decomposition of Mg–RE intermetallic phases by hydrogen during solidification or high-temperature heat treatment.[35] In this work, although EDS analysis cannot be used for detection of the hydrogen element, the cuboid phase is most likely the GdH_2 phase, with part of Gd atoms being replaced by Mg.

The TEM-EDS results also revealed that the Mg matrix in the alloy contains about 0.7 at pct Gd. According to the binary Mg–Gd which is not well established at low temperatures,[36] Gd has only a limited solubility in Mg at room temperature. Therefore, it appears that a state of supersaturated solid solution (SSSS) was formed in the Mg matrix.

To study the optimum ECAP temperature, ECAP was attempted at low temperatures but the material showed insufficient formability at 473 (200 ^{o}C) and 573 K (300 ^{o}C) with cracking occurring after only 1 pass. By increasing the temperature to 623 K (350 ^{o}C), the ductility of the material increased to an acceptable level and 2, 4 and 8 ECAP passes were possible. The microstructure of the material after 2 ECAP passes at 623 K (350 ^{o}C) is shown in Figures 5(a) and (b). As can be observed, the material shows more uniform and smaller grain sizes by comparison with the extruded condition. The average grain size is about 5.0 ± 0.5 μm after 2 ECAP passes at 623 K (350 ^{o}C). Therefore, 623 K (350 ^{o}C) was identified as the optimum ECAP temperature for grain refinement of the GW50 alloy, since formability is insufficient at lower temperatures and grain growth becomes significant at higher temperatures. The optimal ECAP temperature of 623 K (350 ^{o}C) for the present alloy is higher than the temperature of ~473 K (200 ^{o}C) associated with the ECAP processing of conventional magnesium alloys such as AZ31,[37,38] probably because of the high strength of Mg-Gd alloys at lower temperatures[39] and the low diffusion rate of Gd in Mg[40] which retards recrystallization. After determining the optimum ECAP temperature, attempts were made to process samples with more ECAP passes in order to investigate the resultant grain refinement. The microstructures after 4 and 8 ECAP passes are shown in Figures 5(c), (d) and 5(e), (f) where the average grain sizes are about 3.5 and 4.5 ± 0.5 μm, respectively. It seems that increasing the number of passes from 2 to 4 results in a more uniform structure with smaller grain sizes but there is some grain growth after increasing to 8 passes.

EBSD orientation maps of the material after extrusion and ECAP are shown in Figure 6 where the extrusion direction and ECAP axis are normal to the plane of the image. It is apparent that some large grains are present in the microstructure of the alloy after extrusion and these grains may have remained from the deformation state. The orientation maps after different numbers of ECAP passes in Figure 6 demonstrate more clearly that the most refined and uniform

179 microstructure can be obtained after 4 passes. As can be seen in Figure 6(a), the microstructure
180 of the material after extrusion is not uniform and some large grains together with some fine
181 equiaxed grains are present. Accordingly, it seems that partial dynamic recrystallization (DRX)
182 produces a non-uniform microstructure in the extruded sample. The elongated grains in the
183 extruded sample are close to blue in color and the $\{01\bar{1}0\}$ planes are aligned perpendicular to the
184 ED in these grains.The pole figures in Figures 7(a) and (b) show there is no specific basal texture
185 in the material after extrusion. Nevertheless, the $\{01\bar{1}0\}$ planes show a weak texture with a
186 maximum intensity of around 3.7 MRD which probably arises from the grains remaining in the
187 deformed state whereas the DRX grains show a weak randomized texture. Texture of the
188 extruded sample is explained in more detail in another report.[41] On the other hand, more
189 uniform grain sizes can be obtained after processing with ECAP, which suggests the occurrence
190 of complete recrystallization in this condition. Pole figures of the material after 2, 4 and 8 ECAP
191 passes, shown in Figures 7(c), (d), (e), (f), (g), and (h), indicate that, contrary to the extruded
192 sample, a basal texture is formed in these samples. The (0001) planes appear to have rotations of
193 about 50° with respect to the extrusion direction. The different textures and grain sizes obtained
194 by ECAP processing can greatly affect the mechanical properties such as the strain rate
195 sensitivity and superplasticity as discussed in more detail in the following sections.
196
197 *B. Superplastic behavior after optimum ECAP conditions*
198 Since fine-grained materials are susceptible to exhibiting superplastic behavior at elevated
199 temperatures, shear punch tests were performed on the samples processed under the optimum
200 ECAP conditions for grain refinement (4 passes at 623 K (350 ^{o}C)) in order to evaluate the
201 superplastic behavior of the material in the investigated range of temperature and shear strain
202 rate. The SPT curves of the material are shown in Figure 8 where the shear stress is plotted
203 against the normalized displacement for samples processed through 4 passes at 623 K (350 ^{o}C)

and then tested at 623 K (350 °C) in SPT using a range of shear strain rates from 1.7×10^{-2} to 1.3×10^{-1} s^{-1}. The ultimate shear strength (USS, τ_m) can be obtained from these curves and then used to calculate the strain rate sensitivity.

To evaluate the strain rate sensitivity of a material based on the variations of strength with strain rate, and for the case of hot shear deformation, the high temperature shear flow stress, τ, is related to the shear strain rate, $\dot{\gamma}$, by a modified power–law relationship of the form[11]

$$\left(\frac{\dot{\gamma}T}{G}\right) = \left(\frac{Ab}{k}\right)\left(\frac{b}{d}\right)^{p}\left(\frac{\tau}{G}\right)^{\frac{1}{m}} \exp\left(\frac{-Q}{RT}\right) \quad (2)$$

where A is a material parameter, b is the Burgers vector, k is Boltzmann's constant, d is the grain size, p is the inverse grain size exponent, G is the shear modulus, m denotes the strain rate sensitivity index, Q is the deformation activation energy, R is the universal gas constant and T is the absolute temperature. From experimental data for the elastic constants of magnesium, the temperature dependence of the shear modulus is generally expressed as[42]

$$G\ (\text{MPa}) = 19200 - 8.6T\ (\text{K}) \quad (3)$$

Due to the constancy of Q at a given temperature, it is possible to determine the value of m from the simple relationship:

$$m = \left(\frac{\partial \ln(\frac{\tau}{G})}{\partial \ln(\frac{\dot{\gamma}T}{G})}\right)_T \quad (4)$$

Figure 9 shows the variations of the normalized USS of the material plotted against the temperature-compensated shear strain rate for different testing temperatures. According to Eq. (4), the slopes of these curves give the corresponding values of m as listed in Figure 9. It is apparent that the dependency of USS on strain rate is linear at 623 (350 °C) and 673 K (400 °C) with $m \approx 0.26 \pm 0.03$ and 0.30 ± 0.04, respectively. However, the dependency becomes sigmoidal with three distinct regions at 723 K (450 °C) and the region with maximum slope has $m \approx 0.47 \pm 0.05$ through a narrow range of shear strain rates. This slope changes again to linear

with $m \approx 0.25 \pm 0.03$, after increasing the temperature to 773 K (500 ^{o}C). To obtain a better representation of the data, the variation of m with test temperature is plotted in Figure 10. It is obvious from this plot that a maximum strain rate sensitivity index is achieved at 723 K (450 ^{o}C) where $m \approx 0.47 \pm 0.05$.

In order to investigate the severity of grain growth at high temperatures, and also to obtain a better understanding of the microstructural changes during SPT at different temperatures, the microstructures of the material after SPT at 723 K (450 ^{o}C) and 773 K (500 ^{o}C) with strain rate of 1.3×10^{-1} s^{-1} are shown in Figure 11(a), (c), (e) and 11(b), (d), (f), respectively. These microstructures were taken from different areas of the SPT samples and at different magnifications in order to show the microstructural evolution in different regions including both areas associated with most deformation (illustrated schematically as region *B* in Figure 12) and areas without any deformation inside the die area (as in region *A* in Figure 12). The results indicate that severe grain growth occurs at 773 K (500 ^{o}C) by comparison with 723 K (450 ^{o}C). Also, much smaller grain sizes exist in the deformation area by comparison with the die area especially for the sample tested at 723 K (450 ^{o}C). This fact demonstrates the occurrence of dynamic recrystallization as a result of the shear deformation in the deformation area. The combination of temperature and strain rate (in region II of the sigmoidal curve, where the material showed maximum SRS) was such that very small grains, in the range of about 5 μm, were formed in the deformation area at 723 K (450 ^{o}C). However, deformation at 773 K (500 ^{o}C) resulted in extensive grain growth in the material. This considerable difference in grain size of the material deformed at 723 K and 773 K is considered as the origin of the observed difference in SRS of the material at these two temperatures. In fact, although DRX occurs at 773 K, the *m*-value would be reduced in comparison with 723 K because of the fast grain growth at this high temperature. Our previous study on the static grain growth of an Mg–9Gd–4Y–0.4Zr alloy also

demonstrated much higher rates of grain growth at 773 K (500 ^{o}C) by comparison with 723 K (450 ^{o}C).[4]

According to Eq. (2), the deformation activation energy can be calculated at constant shear strain rate as:

$$Q = \frac{R}{m}\left(\frac{\partial ln\left(\frac{\tau}{G}\right)}{\partial\left(\frac{1}{T}\right)}\right)_{\frac{\dot{\gamma}T}{G}} \quad (5)$$

Consequently, the normalized USS values were plotted against the reciprocal of temperature at constant temperature-compensated shear strain on a semi-logarithmic scale as shown in Figure 13 in order to calculate the activation energy of the material after 4 ECAP passes at 623 K (350 ^{o}C). Calculations were made in the temperature range of 673 to 773 K (400 to 500 ^{o}C) and the average activation energy was determined as ~110 ± 5 kJ mol^{-1}.

After studying the SRS of the material (processed through 4 ECAP passes) at different temperatures and strain rates to obtain optimum conditions for superplasticity, it is interesting to compare the results with the material processed by 2 ECAP passes in order to explore the role of small differences in the initial grain size on superplasticity. Accordingly, SPT results of the material processed through 2 ECAP passes at 623 K (350 ^{o}C) are presented in Figure 14. It can be observed that the SRS index value is maximum at the middle range of shear strain rates where the *m*-value is about 0.43 ± 0.02.

IV. DISCUSSION

A. Grain refinement during ECAP processing

The results in Figures 1 and 6 demonstrate that partial recrystallization takes place in the extruded condition and this produces a coexistence of fully recrystallized small grains together with large grains which remain from the deformation step. This means that the deformation conditions of the extrusion process (temperature, strain and strain rate) are not suitable for full

recrystallization of the Mg–5Gd–0.4Zr alloy. This is because the RE elements can retard recrystallization[43] due to their small diffusion rates in Mg.[40] It has been reported that strain (the extrusion ratio) plays a critical role in promoting recrystallization in the GW50 alloy and a fully recrystallized microstructure may be obtained using higher extrusion ratios of 19:1[41].[41] This suggests that the recrystallization behavior of these alloys is severely strain-dependent. In addition to the amount of strain during deformation, the mode of deformation may also greatly influence the recrystallization microstructure. Therefore, the effects of ECAP on the microstructure of the alloy were investigated in this investigation. As shown in Figures 5 and 6, the extent of recrystallization changes from partial in the extruded condition to fully recrystallized even after 2 ECAP passes. Increasing the numbers of ECAP passes from 2 to 4 gives a finer microstructure due to the increased strain.

B. Texture evolution during ECAP processing

The crystallographic texture of the grains plays an important role in enhancing the mechanical properties of Mg and its alloys, in addition to the grain size. However, there are only limited reports to date on the texture of Mg–Gd alloys processed by ECAP.[16] Accordingly, texture evolution was studied in the present work to examine the effects of different deformation processes on the orientation of the grains. The texture of the extruded material was discussed in an earlier report[41] and is included here only for making a direct comparison with the ECAP process. The microstructure of the extruded sample consists of some large grains remaining from the deformation step as a result of partial recrystallization with $\{10\bar{1}0\}$ planes aligned perpendicular to the extrusion axis and with some fine recrystallized grains having an almost randomized texture. The first effect of ECAP on the microstructure of the alloy is to increase the uniformity of the microstructure. Contrary to an earlier report on the microstructure of Mg–Gd alloys processed by ECAP,[16] a uniform microstructure was obtained even after 2 passes and

300 there were no indications of non-uniformity or large grains remaining in the unrecrystallized
301 state. Hence, the texture of the material changed to a basal texture with the (0001) planes aligned
302 in a 50 to 60° angle with respect to the extrusion direction. This texture was reported previously
303 for other magnesium alloys processed by ECAP[44] since the basal planes in the majority of
304 grains become realigned to the shearing direction due to the simple shear applied to the material
305 at the intersection of the channels during ECAP. However, the maximum intensity is smaller
306 than the values reported for other magnesium alloys without RE elements. For example, a
307 maximum intensity of 54 MRD was reported for the AZ31 alloy[45] which is much higher than
308 the maximum intensity of 8.8 MRD obtained in this study for the material processed through 4
309 ECAP passes. This difference probably arises from the role of the RE elements in activating the
310 non-basal slip systems.[46]
311
312 *C. Superplasticity*
313 Fine-grained materials generally exhibit superplastic behavior at high temperatures in
314 addition to their high strength at low temperatures. In this investigation, after determining the
315 optimum ECAP conditions for grain refinement of 4 passes at 623 K (350 ^{o}C), shear punch tests
316 were performed on this material at different temperatures to evaluate the advent of
317 superplasticity using an indirect procedure for measuring the SRS by SPT. Superplasticity is
318 associated with a high resistance to flow instability and is characterized by high *m*-values$\geq$
319 0.5.[15,47] The SPT results indicate that the material processed under the optimum ECAP
320 conditions has a uniform fine-grained microstructure with an average grain size of ~3.5 μm and
321 it is capable of showing superplastic behavior at 723 K (450 ^{o}C) and over a narrow range of
322 shear strain rates. Measurements of the SRS show that the *m*-value increases from an initial
323 value of ~0.26 ± 0.03 at 623 K (350 ^{o}C) to ~0.47 ± 0.05 at 723 K (450 ^{o}C) and then there is a
324 further decrease at higher temperatures. The results confirm that temperatures lower than ~723 K

(450 °C) are not suitable for superplastic deformation. This is because superplasticity is associated with the occurrence of grain boundary sliding (GBS)[48,49] and this requires the diffusion and redistribution of alloying elements during high temperature deformation. As a result, it is reasonable to anticipate that, because of the low diffusion rates of Gd in the Mg matrix,[40] these lower deformation temperatures are not suitable for superplastic deformation in this alloy.

Grain size also plays a critical role in determining the optimum temperature for superplasticity. It is expected that smaller grain sizes will decrease the optimum temperature due to the increased diffusion rate. In this respect, it was reported that the optimum temperature for superplasticity of a nano-grained Mg–9Gd–4Y–0.4Zr alloy processed by HPT was 623 K (350 °C)[14] which is about one hundred degrees lower than the optimum temperature in this study for the fine-grained Mg–5Gd–0.4Zr alloy processed by ECAP. The observed decrease in the *m*-value at higher temperatures above 723 K (450 °C) is due to an inherent grain growth of the fine-grained structure as demonstrated in Figure 11. It was also shown that extensive grain growth occurs both within the deformation and die areas at 773 K (500 °C) by comparison with 723 K (450 °C).

To investigate the deformation mechanism of the material in the superplastic region, it is necessary to consider both the activation energy and the strain rate sensitivity index. The *m*–value of ~0.50 is associated with grain boundary sliding[49] and the activation energy of ~110 ± 5 kJ mol^{-1} is close to the activation energy of ~92 kJ mol^{-1} for grain boundary diffusion in magnesium.[50] Observed differences between the activation energy of the material in this investigation and the value reported for grain boundary diffusion in Mg arises from the lower SRS values at 673 (400 °C) and 773 K (500 °C) which are accompanied by deformation mechanisms other than GBS. It is concluded, therefore, that GBS accommodated by grain boundary diffusion is the dominant deformation mechanism of the Mg–5Gd–0.4Zr alloy in the

superplastic region. This conclusion is consistent with the fine-grained microstructure and the sigmoidal dependence of the SRS on the shear strain rate.

Although the optimum ECAP condition with the most uniform microstructure and the smallest grain sizes were achieved after 4 ECAP passes, the SPT results showed that the SRS of the material after 2 ECAP passes was not greatly different from the SRS of the material processed by 4 ECAP passes. In this respect, the maximum *m*-values of about 0.43 and 0.47 obtained at 723 K (450 °C) for the material processed through 2 and 4 ECAP passes at 623 K (350 °C), respectively, demonstrate that small changes in the initial grain size of the material do not play a crucial role for the subsequent occurrence of superplasticity. It should also be noticed that, in addition to grain size, another important difference between the microstructures of the material processed through 2 and 4 ECAP passes is the distribution of grain orientations which were revealed in the EBSD results (Figures 6 and 7). As discussed in the previous session, although the preferred orientation of grains is almost similar after 2 and 4 passes, it appears that a larger fraction of grains have been sheared during ECAP in the material processed through 4 passes. However, similar to the effect of initial grain size, it seems that this initial texture difference also has little effect on the SRS of the material when comparing the SPT results of the material processed through 2 and 4 ECAP passes.

V. SUMMARY AND CONCLUSIONS

Microstructural and textural evolution of an Mg–5Gd–0.4Zr alloy was investigated by SEM, TEM and EBSD in the extruded and ECAP conditions and the optimum ECAP conditions for grain refinement were determined. Shear punch tests were performed on the material processed under these optimum conditions for evaluation of superplasticity. The following results were achieved.

1. The material shows a non-uniform grain size distribution in the extruded condition consisting of both coarse and fine grains.

2. The optimum temperature for ECAP is 623 K (350 ^{o}C) since the formability is insufficient at lower temperatures and extensive grain growth occurs at higher temperatures.

3. The material has average grain sizes of ~5.0, ~3.5 and ~4.5 ± 0.5 μm after 2, 4 and 8 ECAP passes, respectively. Therefore, 4 passes was chosen as the optimum condition.

4. The SPT results indicate that a maximum strain rate sensitivity index of ~0.47 is achieved at 723 K (450 ^{o}C) and a further increase in temperature leads to a lower value of *m*.

5. The SRS index of ~0.47 and activation energy of ~110 kJ mol^{-1}suggests that the flow mechanism in the superplastic region is grain boundary sliding.

6. The slight differences between the initial grain size and texture of the material processed through 2 and 4 ECAP passes does not play a crucial role for the subsequent occurrence of superplasticity at 723 K (450 °C).

Acknowledgment

The authors thank the Iran National Science Foundation (INSF) for support of this work under Grant no. 94013486.

REFERENCES

[1] B.L. Mordike and T. Ebert: *Mater. Sci. Eng.*, 2001, vol. 302A, pp. 37–45.

[2] M. Kawasaki and T.G. Langdon: *J. Mater. Sci.*, 2016, vol. 51, pp. 19–33.

[3] J. Cizek, I. Prochazka, B. Smola, I. Stulikova, R. Kuzel, Z. Matej, V. Cherkaska, R.K. Islamgaliev and O. Kulyasova: *Mater. Sci. Eng.*, 2007, vol. 462A, pp. 121–26.

[4] R. Alizadeh, R. Mahmudi, A. H. W. Ngan and T. G. Langdon: *J. Mater. Sci.*, 2015, vol. 50, pp. 4940–51.

[5] X. Zhang, L. Li, Y. Deng, and N. Zhou: *J. Alloys Compd.*, 2009, vol. 481, pp. 296–300.

[6] L. Li, X. Zhang, Y. Deng and C. Tang: *J. Alloys Compd.*, 2009, vol. 485, pp. 295–99.

[7] D.J. Li, Q.D. Wang, J.J. Blandin, M. Sueryc, J. Dong and X.Q. Zeng: *Mater. Sci. Eng.*, 2009, vol. 526A, pp. 150–55.

[8] L. Li, X. Zhang, C. Tang, Y. Deng and N. Zhou: *Mater. Sci. Eng.*, 2010, vol. 527A, pp. 1266–74.

[9] Q. Yang, B.L. Xiao and Z.Y. Ma: *J. Alloys Compd.*, 2013, vol. 551, pp. 61–66.

[10] Q. Yang, B.L. Xiao, Q. Zhang, M.Y. Zheng and Z.Y. Ma: *Scr. Mater.*, 2013, vol. 69, pp. 801–04.

[11] R. Alizadeh, R. Mahmudi and T.G. Langdon: *J. Mater. Res. Technol.*, 2014, vol. 3, pp. 228–32.

[12] A. Movahedi-Rad, R. Mahmudi, G.H. Wu and H.R. Jafari-Nodooshan: *J. Alloys Compd.*, 2015, vol. 626, pp. 309–13.

[13] M. Sarebanzadeh, R. Roumina, R. Mahmudi, G.H. Wu and H.R. Jafari-Nodooshan: *Mater. Sci. Eng.*, 2015, vol. 646A, pp. 249–53.

[14] R. Alizadeh, R. Mahmudi, A.H.W. Ngan and T.G. Langdon: *Mater. Sci. Eng.*, 2016, vol. 651A, pp. 786–94.

[15] T.G. Langdon: *J. Mater. Sci.*, 2009, vol. 44, pp. 5998–6010.

[16] F. Zhang, K. Zhang, C. Tan, X. Yu, H. Ma, F. Wang and H. Cai: *Trans. Nonferrous Met. China*, 2011, vol. 21, pp. 2140–46.

[17] J. Zhang, Z. Kang and L. Zhou: *Mater. Sci. Eng.*, 2015, vol. 647A, pp. 184–90.

[18] R. Mahmudi, R. Alizadeh and A.R. Geranmayeh: *Scr. Mater.*, 2011, vol. 64, pp. 521–24.

[19] R. Mahmudi, H. Mahjoubi and P. Mehraram: *Int. J. Mod. Phys. B*, 2008, vol. 22, pp. 2823–32.

[20] R. Mahmudi, R. Alizadeh and S. Azhari: *Mater. Lett.*, 2013, vol. 97, pp. 44–46.

[21] M. Karami and R. Mahmudi: *Mater. Sci. Eng.*, 2013, vol. 576A, pp. 156–59.

[22] N. Fakhar, F. Fereshteh-Saniee and R. Mahmudi: *Mater. Des.*, 2015, vol. 85, pp. 342–48.

[23] M. Furukawa, Y. Iwahashi, Z. Horita, M. Nemoto and T.G. Langdon: *Mater. Sci. Eng.*, 1998, vol. 257A, pp. 328–32.

[24] Y. Iwahashi, J. Wang, Z. Horita, M. Nemoto and T.G. Langdon: *Scr. Mater.*, 1996, vol. 35, pp. 143–46.

[25] R. Alizadeh and R. Mahmudi: *Mater. Sci. Eng.*, 2010, vol. 527A, pp. 3975–83.

[26] G.L. Hankin, M.B. Toloczko, K.I. Johnson, M.A. Khaleel, M.L. Hamilton, F.A. Garner, R.W. Davies and R.G. Faulkner: ASTM STP 1366, 2000, pp. 1018–28.

[27] W.J. Park, H. Park, D.H. Kim and N.J. Kim: *Mater. Sci. Eng.*, 1994, vol. 179–180 A, pp. 637–640.

[28] P. Vostry, B. Smola, I. Stulikova, F. Von Buch and B.L. Mordike: *Phys. Status Solidi*, 1999, vol. 175 A, pp. 491–500.

[29] D. Li, Q. Wang and W. Ding: *Mater. Sci. Eng.*, 2006, vol. 428 A, pp. 295–300.

[30] S.M. He, X.Q. Zeng, L.M. Peng, X. Gao, J.F. Nie and W.J. Ding: *J. Alloy Compd.*, 2007, vol. 427, pp. 316–23.

[31] Z. Yang, Z.H. Wang, H.B. Duan, Y.C. Guo, P.H. Gao and J.P. Li: *Mater. Sci. Eng.*, 2015, vol. 631A, pp. 160–65.

[32] K.Y. Zheng, J. Dong, X.Q. Zeng and W.J. Ding: *Mater. Sci. Technol.*, 2008, vol. 24, pp. 320–326.

[33] Y. Yang, L. Peng, P. Fu, B. Hu and W. Ding: *J. Alloys Compd.*, 2009, vol. 485, pp. 245–248.

[34] Q. Peng, Y. Huang, J. Meng, Y. Li and K.U. Kainer: *Intermetallics*, vol. 19, pp. 382–389.

[35] S.M. Zhu, J.F. Nie, M.A. Gibson and M.A. Easton: *Scri. Mater.*, 2014, vol. 77, 21–24.

[36] ASM Handbook, Alloy Phase Diagrams, vol. 3, ASM International, USA, 1992.

[37] R.B. Figueiredo and T.G. Langdon: *J. Mater. Sci.*, 2008, vol. 43, pp. 7366–71.

[38] Y. Radi and R. Mahmudi: *Mater. Sci. Eng.*, 2010, vol. 527A, pp. 2764–71.

[39] C. Xu, M.Y. Zheng, S.W. Xu, K. Wu, E.D. Wang, S. Kamado, G.J. Wang and X.Y. Lu, *Mater. Sci. Eng.*, 2012, vol. 547A, pp. 93–98.

[40] S.K. Das, Y.B. Kang, T. Ha and I.H. Jung: *Acta Mater.*, 2014, vol. 71, pp. 164–75.

[41] R. Alizadeh, R. Mahmudi, A.H.W. Ngan and T.G. Langdon: *Adv. Eng. Mater.*, 2016, vol. 18, pp. 1044–1049.

[42] S.S. Vagarali and T.G. Langdon: *Acta Met.*, 1981, vol. 29, pp. 1969–82.

[43] N. Stanford: *Mater. Sci. Eng.*, 2013, vol. 565A, pp. 469–75.

[44] T. Mukai, M. Yamanoi, H. Watanabe and K. Higashi: *Scr. Mater.*, 2001, vol. 45, pp. 89–94.

[45] S.M. Masoudpanah and R. Mahmudi: *Mater. Sci. Eng.*, 2010, vol. 527A, pp. 3685–89.

[46] J.P. Hadorn, K. Hantzsche, S. Yi, J. Bohlen, D. Letzig and S.R. Agnew: *Metall. Mater. Trans. A*, 2012, vol. 43, pp. 1363–75.

[47] R.E. Smallman and A.H.W. Ngan: Modern Physical Metallurgy, 8th Edition, Elsevier, 2014, p. 437.

[48] T.G. Langdon: *Mater. Sci. Eng.*, 1994, vol. 174A, pp. 225–30.

[49] T.G. Langdon: *Acta Metall. Mater.*, 1994, vol. 42, pp. 2437–43.

[50] H.J. Frost and M.F. Ashby: Deformation-Mechanism Maps: The Plasticity and Creep of Metals and Ceramics, Pergamon Press, Oxford, U.K., 1982.

LEGENDS

Fig. 1. (a) SEM micrograph of the alloy after extrusion, and (b) enlarged photo of the dashed area in (a).

Fig. 2. SEM micrograph of the precipitates in the extruded materials, together with SEM-EDS line scan results.

Fig. 3. TEM micrograph of a cuboid precipitate (a) and the corresponding SAED patterns, with zone axis parallel to [001] (b) and [112] (c).

Fig 4. TEM-EDS spectrums of points *A* (a) and *B* (b), with the elemental concentrations of Mg, Gd and Zr (c).

Fig. 5. SEM micrographs of the alloy after 2 (a,b), 4 (c,d) and 8 (e,f) ECAP passes.

Fig. 6. EBSD orientation maps of the alloy after extrusion (a), 2 (b), 4 (c), and 8 (d) ECAP passes.

Fig. 7. Pole figures of the material after extrusion (a,b), 2 (c,d), 4 (e,f) and 8 (g,h) ECAP passes.

Fig. 8. SPT curves of the material after 4 ECAP passes at 623 K (350 ^{o}C).

Fig. 9. Normalized τ_m values of the material after 4 ECAP passes, as a function of temperature-compensated shear strain rate at different temperatures.

Fig. 10. Variations of *m*-value with temperature after 4 ECAP passes.

Fig. 11. SEM micrographs of different areas of the material after SPT at 723 K (450 ^{o}C) (a,c,e) and 773 K (500 ^{o}C) (b,d,f) with strain rate of 1.3×10^{-1} s^{-1}.

Fig. 12. Schematic of the shear punch sample, before and after deformation.

Fig. 13. Temperature dependence of normalized τ_m values at constant temperature-compensated shear strain rates for the material after 4 ECAP passes.

Fig. 14. Normalized τ_m values of the material after 2 ECAP passes, as a function of temperature-compensated shear strain rate at the test temperature of 723 K (450 °C).

Table I. Summary of literature data on the superplasticity of Mg–Gd alloys processed by different methods

Table II. Summary of the localized methods used for evaluation of superplasticity

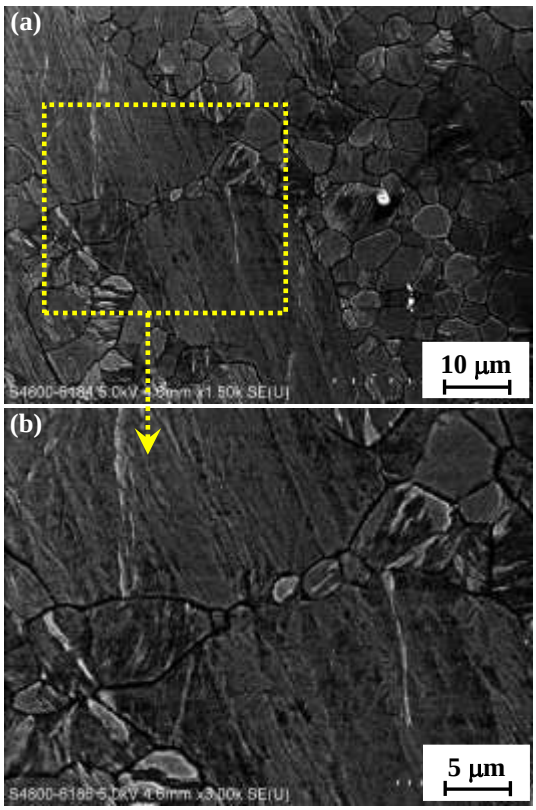

Fig. 1. (a) SEM micrograph of the alloy after extrusion, and (b) enlarged photo of the dashed area in (a).

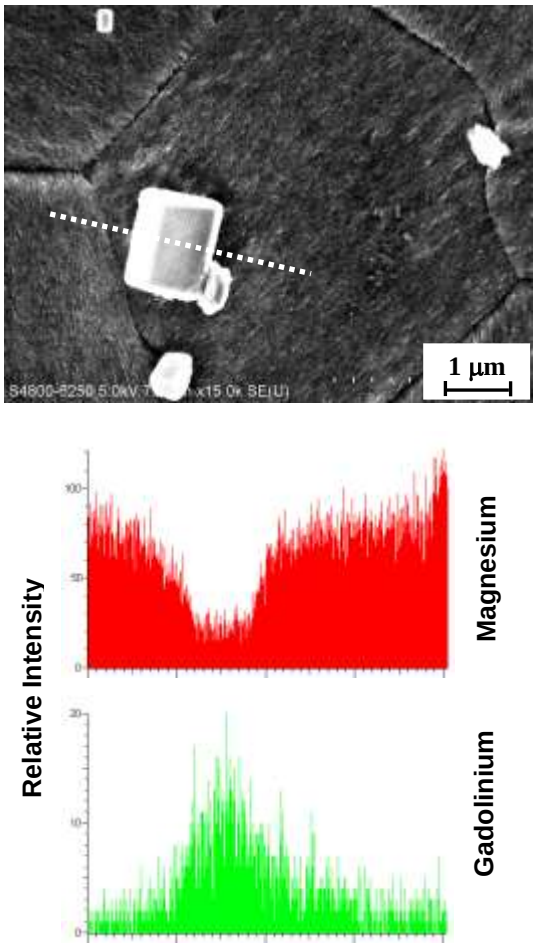

Fig. 2. SEM micrograph of the precipitates in the extruded materials, together with SEM-EDS line scan results.

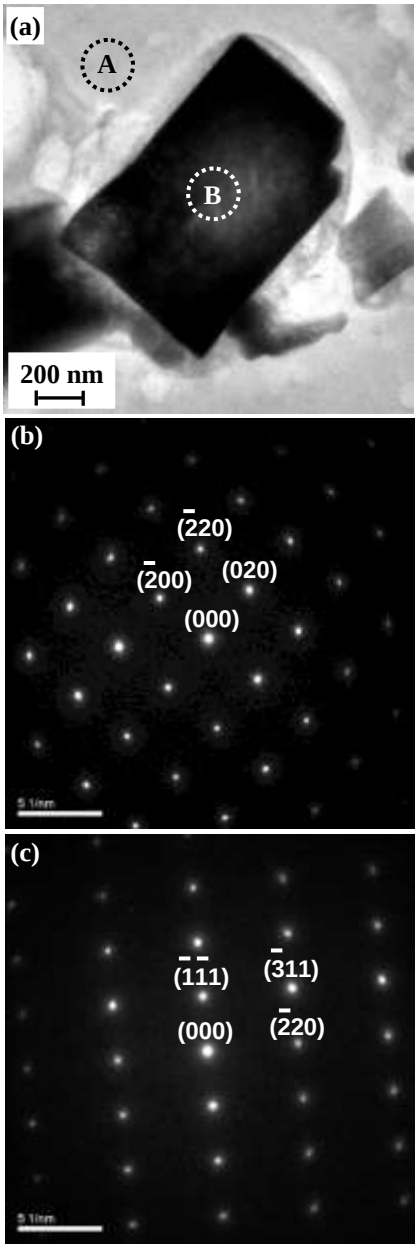

Fig. 3. TEM micrograph of a cuboid precipitate (a) and the corresponding SAED patterns, with zone axis parallel to [001] (b) and [112] (c).

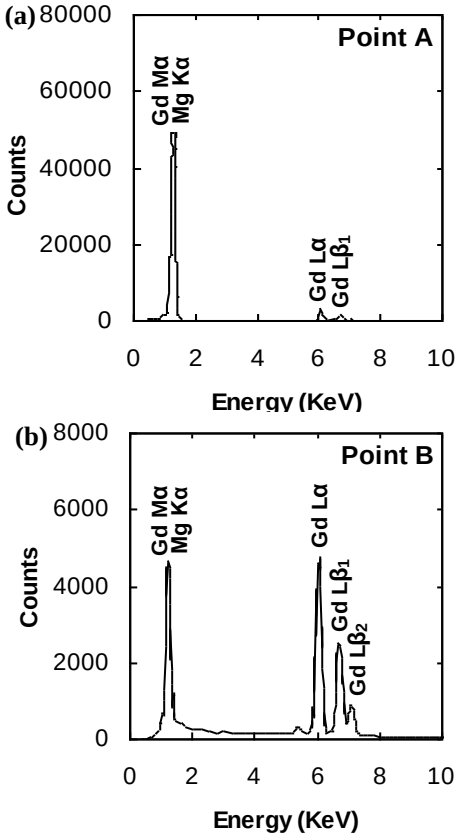

(c)

Element (at. %)	A	B
Mg	99.3	35.5
Gd	0.7	64.5
Zr	0.0	0.0

Fig 4. TEM-EDS spectrums of points *A* (a) and *B* (b), with the elemental concentrations of Mg, Gd and Zr (c).

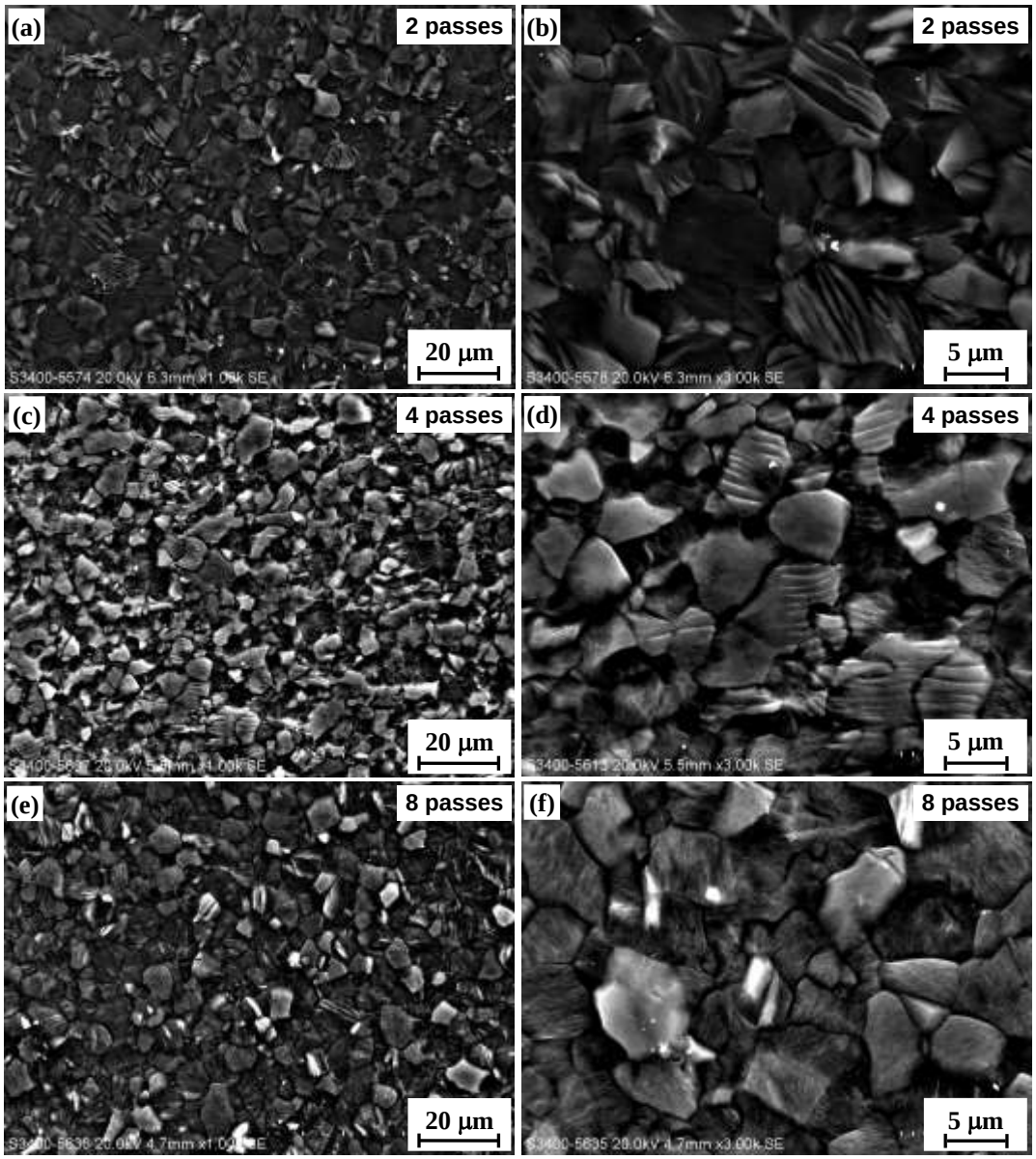

Fig. 5. SEM micrographs of the alloy after 2 (a,b), 4 (c,d) and 8 (e,f) ECAP passes.

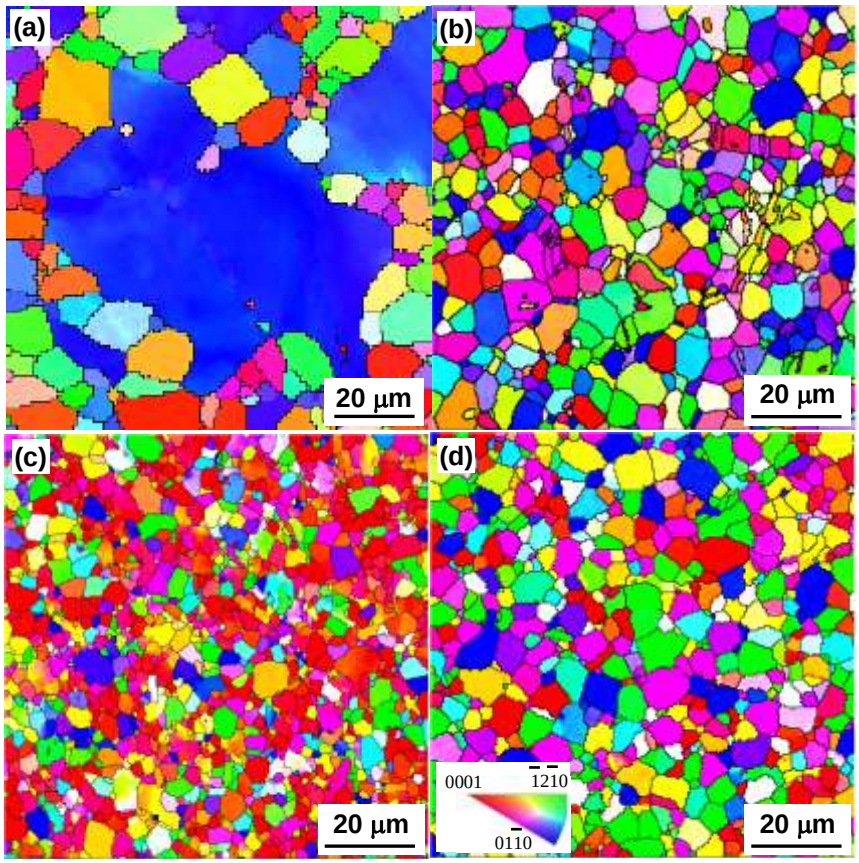

Fig. 6. EBSD orientation maps of the alloy after extrusion (a), 2 (b), 4 (c), and 8 (d) ECAP passes.

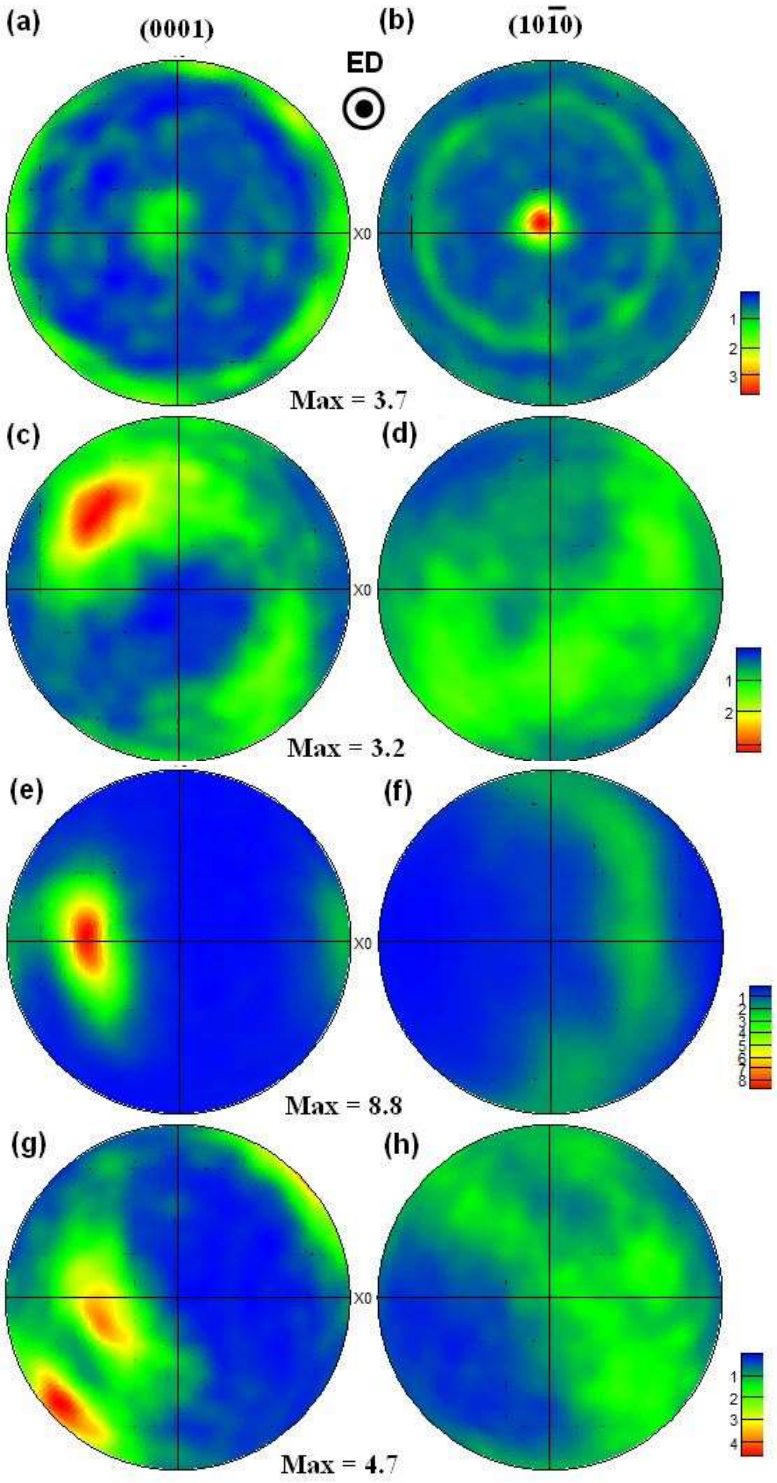

Fig. 7. Pole figures of the material after extrusion (a,b), 2 (c,d), 4 (e,f) and 8 (g,h) ECAP passes.

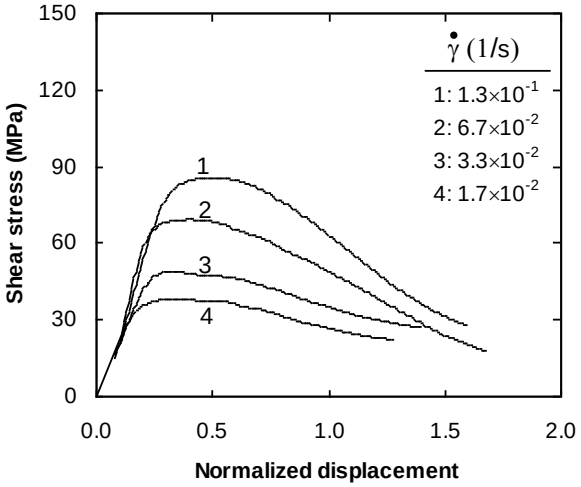

Fig. 8. SPT curves of the material after 4 ECAP passes at 623 K.

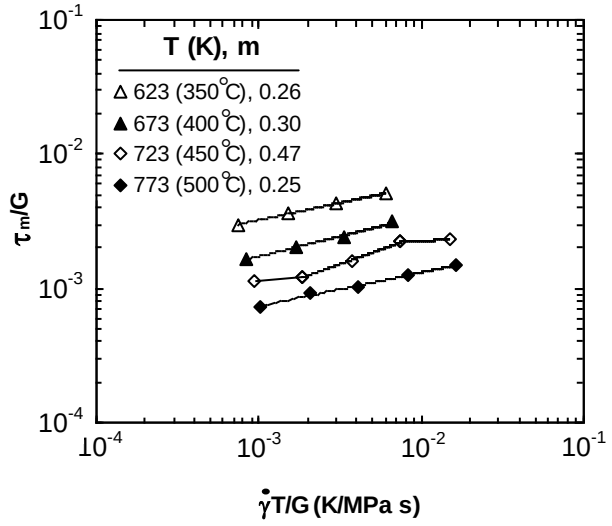

Fig. 9. Normalized τ_m values of the material after 4 ECAP passes, as a function of temperature-compensated shear strain rate at different temperatures.

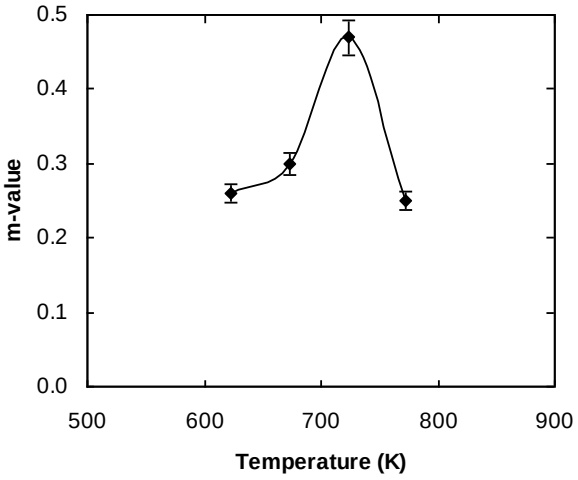

Fig. 10. Variations of *m*-value with temperature after 4 ECAP passes.

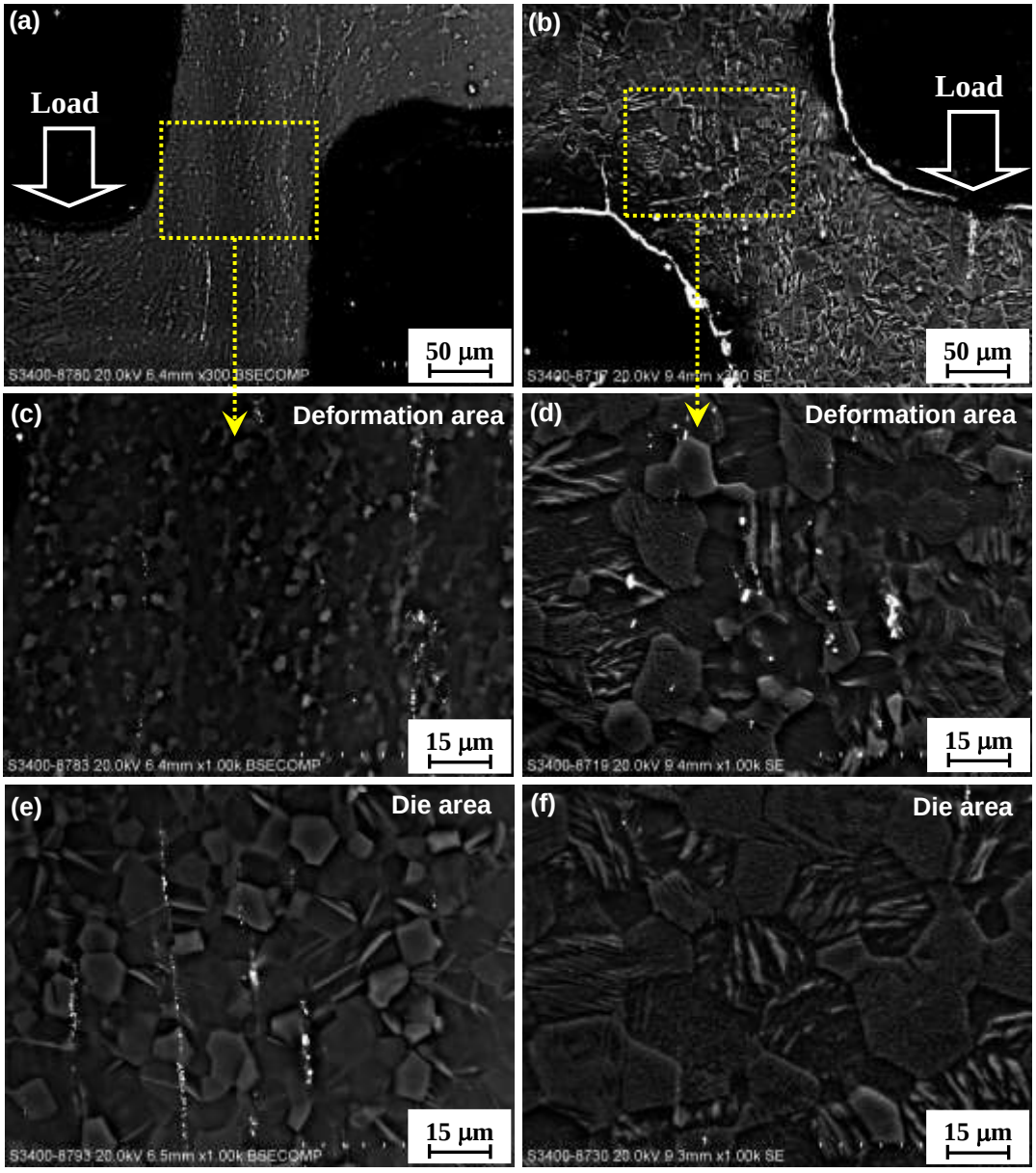

Fig. 11. SEM micrographs of different areas of the material after SPT at 723 K (a,c,e) and 773 K (b,d,f) with strain rate of 1.3×10^{-1} s^{-1}.

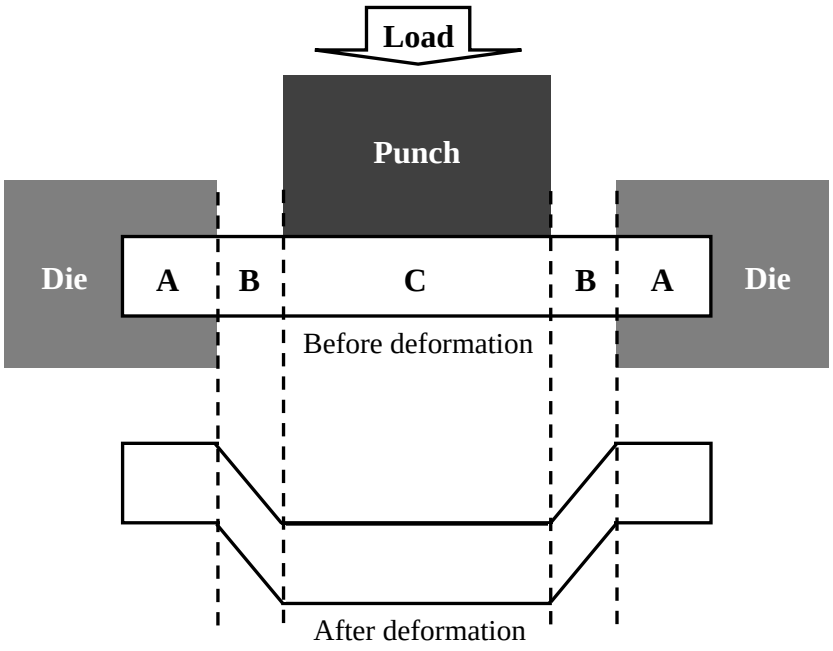

Fig. 12. Schematic of the shear punch sample, before and after deformation.

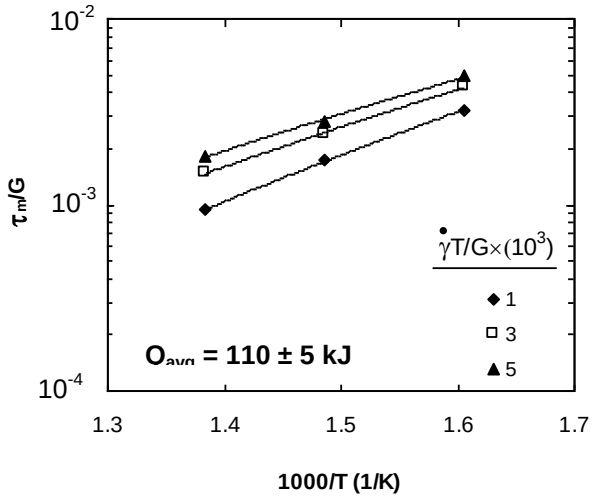

Fig. 13. Temperature dependence of normalized τ_m values at constant temperature-compensated shear strain rates for the material after 4 ECAP passes.

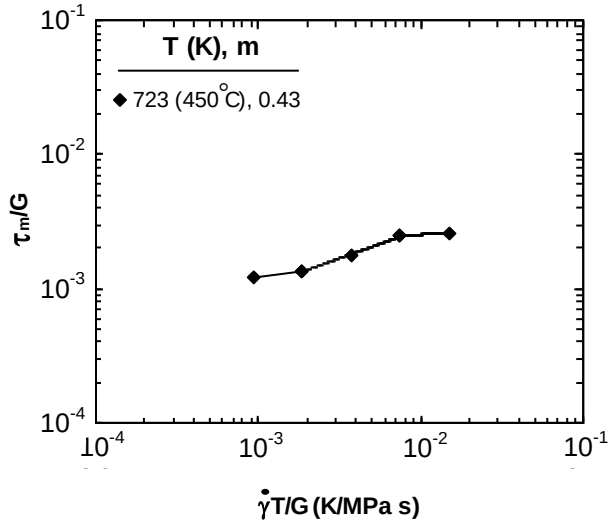

Fig. 14. Normalized τ_m values of the material after 2 ECAP passes, as a function of temperature-compensated shear strain rate at the test temperature of 723 K (450 °C).

Table 1. Summary of literature data on the superplasticity of Mg-Gd alloys processed by different methods

Alloy or Composition (wt%)	SPD		Grain size (μm)	Superplasticity			Reference
	Process	Temperature (K)		Temperature (K)	Maximum elongation (%)	SRS value	
GW94[a]	Extrusion (16:1)	648	10	723	410	0.54	Zhnag et al. [4]
GW94	Rolling	623	66	708	380	0.56	Li et al. [5]
GW83	Extrusion (56:1)	673	11	673	-	0.3	Li et al. [6]
GW94	Rolling	623	120	723	400	0.32	Li et al. [7]
GW103	FSP[b]	298	6.1	688	1110	0.5	Yang et al. [8]
Mg–9.4Gd–4.1Y–1.2Zn–0.4Zr	FSP	298	3	698	3570	0.6	Yang et al. [9]
GW94	Extrusion (19:1)	673	8.6	723	-	0.40	Alizadeh et al. [10]
Mg–8.5Gd–2.5Y–2Ag–0.5Zr	Extrusion (8:1)	673	3	573	-	0.51	Movahedi-Rad [11]
GZ31[c]	EX-ECAP[d]	553	1.7	673	-	0.51	Sarebanzadeh [12]
GW94	HPT	298	0.085	673	-	0.51	Alizadeh et al. [13]

[a] GW94: Mg–9Gd–4Y-0.4Zr.
[b] FSP: Friction stir processing.
[c] GZ31: Mg–3Gd-1Zn.
[d] EX-ECAP: Extrusion+ECAP.

Table 2. Summary of the localized methods used for evaluation of superplasticity

Method	Alloy or composition (wt%)	Fabrication process	Superplasticity		Reference
			Testing temperature (K)	SRS value	
Impression creep	Sn-5Sb	ECAP	298	0.60	Mahmudi et al. [17]
Indentation creep	Sn-1Bi	ECAP	298	0.40	Mahmudi et al. [18]
SPT[a]	Sn-5Sb	ECAP	298	0.57	Mahmudi et al. [19]
SPT	GW94	Extrusion	723	0.40	Alizadeh et al. [10]
SPT	Mg-12Li-1ZZn	ECAP	548	0.45	Karami and Mahmudi [20]
SPT	AA5083[b]	DECLE[c]	673	0.43	Fakhar et al. [21]
SPT	GZ31	ECAP	673	0.51	Sarebanzadeh et al. [12]
SPT	GW94	HPT	673	0.51	Alizadeh et al. [13]

[a] SPT: Shear punch test.
[b] AA5083: Al–4.2%Mg–0.63%Mn–0.18%Fe.
[c] DECLE: Double equal channel lateral extrusion.